Imaging live humans through smoke and flames using far-infrared digital holography

M. Locatelli,[1] E. Pugliese,[1] M. Paturzo,[2] V. Bianco,[2] A. Finizio,[2] A. Pelagotti,[1] P. Poggi,[1] L. Miccio,[2] R. Meucci,[1] and P. Ferraro[2]*

[1]CNR Istituto Nazionale di Ottica—Largo E. Fermi, 6 50125 Firenze, Italy
[2]CNR Istituto Nazionale di Ottica—Sezione di Napoli, Via Campi Flegrei, 34 80078 Pozzuoli (Napoli), Italy
**pietro.ferraro@ino.it*

Abstract: The ability to see behind flames is a key challenge for the industrial field and particularly for the safety field. Development of new technologies to detect live people through smoke and flames in fire scenes is an extremely desirable goal since it can save human lives. The latest technologies, including equipment adopted by fire departments, use infrared bolometers for infrared digital cameras that allow users to see through smoke. However, such detectors are blinded by flame-emitted radiation. Here we show a completely different approach that makes use of lensless digital holography technology in the infrared range for successful imaging through smoke and flames. Notably, we demonstrate that digital holography with a cw laser allows the recording of dynamic human-size targets. In this work, easy detection of live, moving people is achieved through both smoke and flames, thus demonstrating the capability of digital holography at 10.6 μm.

OCIS codes: (090.1995) Digital holography; (110.0113) Imaging through turbid media; (110.3080) Infrared imaging; (040.2235) Far infrared or terahertz; (290.7050) Turbid media.

References and links

1. U.S. Fire Administration, *http://www.usfa.fema.gov/statistics*.
2. G. Zizak, "Flame emission spectroscopy: fundamentals and applications. Lecture given at the ICS training course on laser diagnostics of combustion processes," (NILES, University of Cairo, Egypt, 2000).
3. A. Àgueda, E. Pastor, Y. Pérez, and E. Planas, "Experimental study of the emissivity of flames resulting from the combustion of forest fuels," Int. J. Therm. Sci. **49**(3), 543–554 (2010).
4. G. Parent, Z. Acem, S. Lechêne, and P. Boulet, "Measurement of infrared radiation emitted by the flame of a vegetation fire," Int. J. Therm. Sci. **49**(3), 555–562 (2010).
5. T. Kreis, *Handbook of Holographic Interferometry: Optical and Digital Methods* (Wiley-VCH Verlag GmbH & Co. KGaA, 2005).
6. M. Hÿtch, F. Houdellier, F. Hüe, and E. Snoeck, "Nanoscale holographic interferometry for strain measurements in electronic devices," Nature **453**(7198), 1086–1089 (2008).
7. I. Yamaguchi, T. Ida, M. Yokota, and K. Yamashita, "Surface shape measurement by phase-shifting digital holography with a wavelength shift," Appl. Opt. **45**(29), 7610–7616 (2006).
8. Y. Kikuchi, D. Barada, T. Kiire, and T. Yatagai, "Doppler phase-shifting digital holography and its application to surface shape measurement," Opt. Lett. **35**(10), 1548–1550 (2010).
9. Y. Frauel, A. Castro, T. J. Naughton, and B. Javidi, "Resistance of the double random phase encryption against various attacks," Opt. Express **15**(16), 10253–10265 (2007).
10. O. Mudanyali, D. Tseng, C. Oh, S. O. Isikman, I. Sencan, W. Bishara, C. Oztoprak, S. Seo, B. Khademhosseini, and A. Ozcan, "Compact, light-weight and cost-effective microscope based on lensless incoherent holography for telemedicine applications," Lab Chip **10**(11), 1417–1428 (2010).
11. M. Paturzo, A. Finizio, P. Memmolo, R. Puglisi, D. Balduzzi, A. Galli, and P. Ferraro, "Microscopy imaging and quantitative phase contrast mapping in turbid microfluidic channels by digital holography," Lab Chip **12**(17), 3073–3076 (2012).
12. V. Bianco, M. Paturzo, A. Finizio, D. Balduzzi, R. Puglisi, A. Galli, and P. Ferraro, "Clear coherent imaging in turbid microfluidics by multiple holographic acquisitions," Opt. Lett. **37**(20), 4212–4214 (2012).
13. E. Shaffer, C. Moratal, P. Magistretti, P. Marquet, and C. Depeursinge, "Label-free second-harmonic phase imaging of biological specimen by digital holographic microscopy," Opt. Lett. **35**(24), 4102–4104 (2010).
14. J. Rosen and G. Brooker, "Non-scanning motionless fluorescence three-dimensional holographic microscopy," Nat. Photonics **2**(3), 190–195 (2008).

#181596 - $15.00 USD Received 11 Dec 2012; revised 11 Jan 2013; accepted 15 Jan 2013; published 26 Feb 2013

15. Z. Wang, L. Millet, M. Mir, H. Ding, S. Unarunotai, J. Rogers, M. U. Gillette, and G. Popescu, "Spatial light interference microscopy (SLIM)," Opt. Express **19**(2), 1016–1026 (2011).
16. T. Shimobaba, Y. Sato, J. Miura, M. Takenouchi, and T. Ito, "Real-time digital holographic microscopy using the graphic processing unit," Opt. Express **16**(16), 11776–11781 (2008).
17. V. Mico, Z. Zalevsky, and J. García, "Superresolution optical system by common-path interferometry," Opt. Express **14**(12), 5168–5177 (2006).
18. M. Paturzo, P. Memmolo, A. Finizio, R. Näsänen, T. J. Naughton, and P. Ferraro, "Synthesis and display of dynamic holographic 3D scenes with real-world objects," Opt. Express **18**(9), 8806–8815 (2010).
19. L. Onural, *3D Video Technologies: An Overview of Research Trends* (SPIE, 2010).
20. B. Katz, J. Rosen, R. Kelner, and G. Brooker, "Enhanced resolution and throughput of Fresnel incoherent correlation holography (FINCH) using dual diffractive lenses on a spatial light modulator (SLM)," Opt. Express **20**(8), 9109–9121 (2012).
21. M. S. Heimbeck, M. K. Kim, D. A. Gregory, and H. O. Everitt, "Terahertz digital holography using angular spectrum and dual wavelength reconstruction methods," Opt. Express **19**(10), 9192–9200 (2011).
22. F. Dubois, N. Callens, C. Yourassowsky, M. Hoyos, P. Kurowski, and O. Monnom, "Digital holographic microscopy with reduced spatial coherence for three-dimensional particle flow analysis," Appl. Opt. **45**(5), 864–871 (2006).
23. H. Ding, Z. Wang, F. Nguyen, S. A. Boppart, and G. Popescu, "Fourier transform light scattering of inhomogeneous and dynamic structures," Phys. Rev. Lett. **101**(23), 238102 (2008).
24. M. Paturzo, A. Pelagotti, A. Finizio, L. Miccio, M. Locatelli, A. Gertrude, P. Poggi, R. Meucci, and P. Ferraro, "Optical reconstruction of digital holograms recorded at 10.6 microm: route for 3D imaging at long infrared wavelengths," Opt. Lett. **35**(12), 2112–2114 (2010).
25. E. Stoykova, F. Yaraş, H. Kang, L. Onural, A. Geltrude, M. Locatelli, M. Paturzo, A. Pelagotti, R. Meucci, and P. Ferraro, "Visible reconstruction by a circular holographic display from digital holograms recorded under infrared illumination," Opt. Lett. **37**(15), 3120–3122 (2012).
26. A. Pelagotti, M. Locatelli, A. Geltrude, P. Poggi, R. Meucci, M. Paturzo, L. Miccio, and P. Ferraro, "Reliability of 3D imaging by digital holography at long IR wavelength," J. Disp. Technol. **6**(10), 465–471 (2010).
27. E. Allaria, S. Brugioni, S. De Nicola, P. Ferraro, S. Grilli, and R. Meucci, "Digital holography at 10.6 μm," Opt. Commun. **215**(4-6), 257–262 (2003).
28. M. P. Georges, J.-F. Vandenrijt, C. Thizy, Y. Stockman, P. Queeckers, F. Dubois, and D. Doyle, "Digital holographic interferometry with CO_2 lasers and diffused illumination applied to large space reflector metrology [Invited]," Appl. Opt. **52**(1), A102–A116 (2013).
29. I. Alexeenko, J.-F. Vandenrijt, G. Pedrini, C. Thizy, B. Vollheim, W. Osten, and M. P. Georges, "Nondestructive testing by using long-wave infrared interferometric techniques with CO_2 lasers and microbolometer arrays," Appl. Opt. **52**(1), A56–A67 (2013).
30. P. A. Blanche, A. Bablumian, R. Voorakaranam, C. Christenson, W. Lin, T. Gu, D. Flores, P. Wang, W. Y. Hsieh, M. Kathaperumal, B. Rachwal, O. Siddiqui, J. Thomas, R. A. Norwood, M. Yamamoto, and N. Peyghambarian, "Holographic three-dimensional telepresence using large-area photorefractive polymer," Nature **468**(7320), 80–83 (2010).
31. M. Cho and B. Javidi, "Three-dimensional tracking of occluded objects using integral imaging," Opt. Lett. **33**(23), 2737–2739 (2008).
32. I. N. Papadopoulos, S. Farahi, C. Moser, and D. Psaltis, "Focusing and scanning light through a multimode optical fiber using digital phase conjugation," Opt. Express **20**(10), 10583–10590 (2012).
33. Z. Yaqoob, D. Psaltis, M. S. Feld, and C. Yang, "Optical phase conjugation for turbidity suppression in biological samples," Nat. Photonics **2**(2), 110–115 (2008).
34. M. P. Georges, J.-F. Vandenrijt, C. Thizy, I. Alexeenko, G. Pedrini, and W. Osten, "Speckle interferometry at 10μm with CO2 lasers and microbolometers array," Proc. SPIE **8412**, 84121O (2012).
35. X. Cai and H. Wang, "The influence of hologram aperture on speckle noise in the reconstructed image of digital holography and its reduction," Opt. Commun. **281**(2), 232–237 (2008).
36. J. Maycock, B. M. Hennelly, J. B. McDonald, Y. Frauel, A. Castro, B. Javidi, and T. J. Naughton, "Reduction of speckle in digital holography by discrete Fourier filtering," J. Opt. Soc. Am. A **24**(6), 1617–1622 (2007).
37. J. W. Goodman, *Speckle Phenomena in Optics: Theory and Applications* (Roberts & Company Publishers, 2007), Chap. 5.

1. Introduction and state of art

The possibility of having clear vision in fire scenes is of fundamental importance, and it presents a great challenge in military and homeland security situations. Fire is a cruel and dangerous destroyer, causing thousands of deaths and severe permanent burn injuries every year. In the United States, for example, fire departments respond to about 1.6 million fire calls per year, and domestic house fires make up the majority of them [1] (3000 deaths occurring each year in house fires).

The recent generation of infrared (IR) bolometer detectors, commercially available for imaging in the IR spectrum in the range of 7–14 μm, are uncooled (*i.e.*, they operate without liquid nitrogen), thus they are lighter in weight and have reached high density and resolution

#181596 - $15.00 USD Received 11 Dec 2012; revised 11 Jan 2013; accepted 15 Jan 2013; published 26 Feb 2013

array (680×480 pixels; pixel size down to 25 μm). Also, the cost of such devices is no longer so high, considering their brilliant performance. Such devices allow passive or active clear vision (i.e., with laser IR illumination) through smoke or fog since IR electromagnetic radiation is scattered just slightly by fog drops or smoke particles. However, visible radiation is strongly affected by scattering, and vision can be completely impaired in such situations. Many fire departments use IR cameras based on a bolometer for exploring fire scenes in order to have clearer vision and to allow the rescue of human lives, or to operate safely in such a hostile environment. As explained above, while imaging through smoke is possible in the range of 7–14 μm, flames can completely blind the detector. In fact, electromagnetic radiation emitted by flames can severely saturate the detector, occluding the scene behind them.

On the industrial side, the failure of furnace and boiler equipment can cause quality problems and, in some cases, it can also be serious enough to force the shutting down of an entire process line. Special thermal imaging cameras are often used to detect most equipment problems during operations so that failures can be prevented. These cameras use a spectral waveband filter that only allows the detection of thermal radiation within specific wavelengths. Usually the filter is around 3.80 μm, where no hot gases are emitted. In fact, gases present in flames have discrete absorption bands in the IR spectrum: the maxima for CO^2 are at 2.7, 4.4, and 15 μm; for H^2O they are at 1.4, 1.9, 2.7, 6 and 17 μm. Therefore, thermal imaging cameras equipped with such filters are ideal for furnace inspections but cannot be used to see through all kinds of flames, e.g., in the flames generated during the combustion of a forest or building. In fact, solid particles of incandescent soot emit radiation in a continuous spectrum over a wider region from visible to IR and also at around 3.8 μm. They are considered to behave as gray bodies (absorptivity is independent of wavelength and temperature). The relative contribution of soot radiation and band radiation associated with hot gases depends on flame thickness: for thin flames (<0.20 m) band radiation dominates, whereas the contribution of soot radiation to flame radiation dominates as flame thickness increases. Another contribution to the continuous spectrum comes from the burning of vegetation, which emits in a stronger and more continuous way in the IR region. In other cases, the continuous spectral emission of flames may be due to processes such as recombination of ions or associations of atoms and radicals [2–4].

Here we demonstrate a different approach to through-flame imaging based on an interferometric technique, i.e., digital holography [5] (DH). In recent years, both holography and DH have been seen as a considerable step forward and have been applied in many fields of science and technology—as a powerful and flexible tool for shape and strain measurements [6–8], for optical-image encryption [9], for quantitative analysis of biological samples [10–15], in real-time modality with good resolution [16,17], and in 3D imaging and display [18,19] using a wide range of experimental setups and light sources [20–23], e.g., Long-IR-DH [24–29].

Recently, a holo-stereographic technique has been used to get a dynamic display of live people by making use of a pulsed laser source and a photorefractive polymer as a recording medium [30]. In our research, we employ a cw laser and a simple user-friendly IR sensor to acquire human-size holograms that can be numerically reconstructed or displayed in quasi real time. In addition, the need of imaging methods for discovering occluded objects [31] or seeing in scattering media is of fundamental importance in many fields, from security to biotechnology and microfluidics [11,12,32,33] (i.e., imaging in tissue or biological fluids).

In this work, two challenging objectives have been achieved, thanks to lensless DH at far IR:

- Real-time recording of live, moving people by cw laser.
- Clear imaging through smoke and flames, independent from the chemical nature of the burning materials involved and from their emission spectrum. Therefore, the proposed approach can be applied to all kind of flames.

The combination of both these capabilities, which is not achievable by any other imaging technique, provides a unique possibility to perform real-time dynamic detection of moving

#181596 - $15.00 USD Received 11 Dec 2012; revised 11 Jan 2013; accepted 15 Jan 2013; published 26 Feb 2013

people in fire scenes. Figure 1 shows a sketch of a typical fire scene, with people trapped in an apartment invaded by smoke and flames. This is a case where the naked-eye vision is completely impaired and the rescue operations slow down. In this case, a thermographic camera would not be able to return a full view of the people inside the apartment because of flame emissions. However, the holographic view would be able to discard both the smoke and the flame contribution and offer a very clear view of any people behind them, providing a potential innovative application in the safety field. The IR-DH holographic system could be mounted on a tripod (see also figures in [34]).

This work is organized as follows. In Section 2 we discuss the advantages of lensless IR-DH and the setup used in our experiments is described. In Section 3 we describe the experiments carried out to demonstrate the holographic capability of imaging objects and human-size targets through smoke and flames. Finally, in Section 4 some conclusions are drawn.

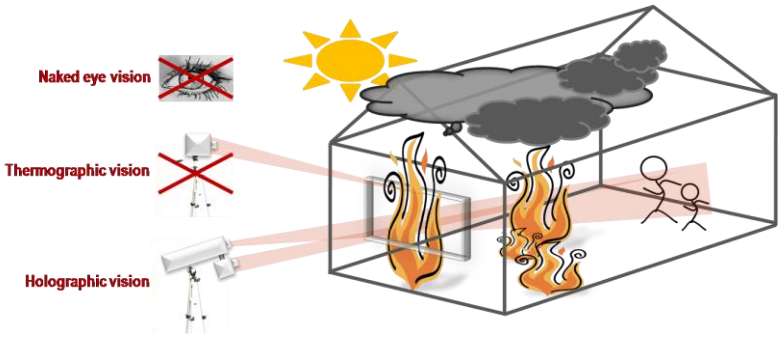

Fig. 1. Sketch of a typical fire scenario where the line of sight is impaired by smoke and flames. Both the naked-eye vision and the thermographic view are blinded by flame emission. Holography at IR can allow clear vision.

2. Working principle: lensless IR-DH

DH at a long IR wavelength has considerable advantages that make it very flexible and useful for recording real-world, large scenes as follows:

- Thanks to the long wavelength, it is possible to record digital holograms of human-size objects.
- Hologram recording can be realized in open space and in daylight conditions, thus allowing this technology to be brought out of the laboratory.
- A longer wavelength makes the recording of an interference pattern (the hologram) much less sensitive to vibrations.
- High-power CO^2 laser sources are broadly available with good coherent properties, so it is possible to expand the object beam to view very large scenes.
- DH allows one to employ a lensless setup to perform out-of-focus acquisitions. Indeed, digital techniques are available to reconstruct the object wave field in the focus plane. In this way the typical saturation of the IR camera elements can be avoided and the sensor is not blinded by the flame emission.

These features of IR-DH provide an opportunity to take an important step forward to achieve clear imaging of a real-world large scene. In fact, here we show that IR-DH has real potential to be used in real-world fire-scenarios in order to get clear vision through smoke and flames.

Indeed, as we show in the following, IR-DH allows us not only to record objects immersed in smoke but also to visualize objects behind flames. Conversely, we show how a live moving

#181596 - $15.00 USD Received 11 Dec 2012; revised 11 Jan 2013; accepted 15 Jan 2013; published 26 Feb 2013

body behind the flames cannot be detected by simple imaging with the same IR camera, while IR holography can do it.

In order to demonstrate this unique imaging potential, two kinds of experiments were conducted where the capability of seeing through smoke and flames by IR-DH were tested.

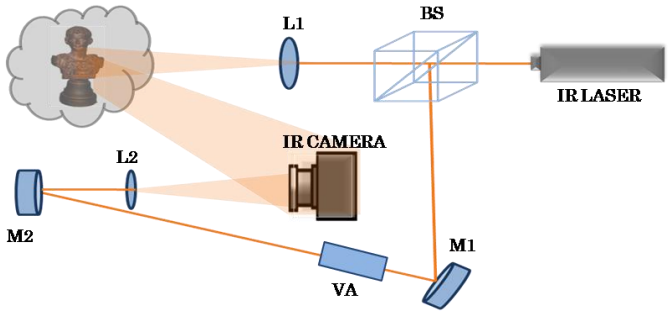

Fig. 2. Experimental set-up: interferometric set-up in lensless off-axis configuration. (BS): beam splitter. (L1, L2): lenses. (VA): variable attenuator. (M1, M2): mirrors.

In Fig. 2 we show the system adapted to image a metallic object placed in a sealed Plexiglas™ chamber (for safety reasons). The optical setup is a typical interferometric setup in a lensless off-axis configuration with a long-IR laser source. The laser used throughout our experiments is a CO^2 laser, Blade 100 by EL.EN Spa, emitting linearly polarized radiation at 10.59 μm relative to the line P(20) in continuous mode on the Gaussian fundamental TEM00 mode up to a maximum power of 110 W; the laser beam was characterized by a minimum diameter beam waist at the output of the resonant cavity of about 10 mm and a divergence of about 2.2 mrad. The CO^2 laser beam is first divided by a ZnSe beam splitter (BS) which reflects 80% of the impinging radiation and transmits the remaining 20%. The transmitted part, which constitutes the reference beam, is reflected by means of a plane mirror (M1) toward a ZnSe variable attenuator (VA); the reference beam is then redirected by means of another plane mirror (M2) toward the thermocamera but, before impinging on the detector, it encounters a ZnSe converging lens of 1.5 inch focal length (L2), which focuses and then enlarges it in order to reach the thermocamera with enough low intensity and an almost planar wavefront. The reflected part of the fundamental beam constitutes the object beam; before impinging on the sample, it passes through a ZnSe converging lens of 1.5 inch focal length (L1), which focuses and then enlarges the beam so as to irradiate a more-or-less large surface of the object depending on its distance from the sample. The interference pattern created by the object beam and the reference beam across the sensor is optimized in order to increase the fringe visibility by acting on the reference beam intensity by means of the variable attenuator. The hologram can be collected and digitally stored in a computer, both in the form of a single image and in the form of a video, if a dynamic scene is of interest. The detector used throughout our experiments was a micro-bolometric camera (640×480 array) by Thermoteknix Miricle, with a frame rate of 50 frame/s, a pixel pitch of 25 μm×25 μm, and a spectral response in the range 8 μm–12 μm.

Thanks to the low sensitivity to vibrations of the whole system, the anti-vibration modality of the table is not activated during the experiments. Since the detector is only sensitive to IR radiation, artificial lights or sunlight are not disruptive. It is necessary to vary the inclination between the object and the reference beam so as to obtain a sufficiently high fringe spatial frequency to separate the real image from the virtual one without breaking the limits imposed by the sampling theorem.

As will be discussed in the following sections, the recorded holograms have been reconstructed by means of the Fresnel method, the diffraction orders out of interest have been filtered, and a numerical enhancement has been performed to improve the image quality.

#181596 - $15.00 USD Received 11 Dec 2012; revised 11 Jan 2013; accepted 15 Jan 2013; published 26 Feb 2013

3. Experimental results

3.1 Seeing through smoke

Here we show the results of the first experiment carried out to show the holographic capability of imaging a metal object through very dense smoke. In order to obtain high enough smoke density around the target, we set it inside a sealed Plexiglas™ box where incense was burning. We used a small bronze statue 10 cm high as a target. On one side of the box two windows in the IR range were opened—an AR/AR ZnSe input window through which the laser beam can reach the object and a germanium output window through which the light diffused by the object can reach the thermal camera detector, whose distance from the object is 25 cm. In order to obtain a quantitative measurement of the smoke concentration inside the box, we evaluated the attenuation of the radiation intensity of a 15 mW laser diode traveling for 6 cm inside the box before reaching a Si photodiode connected to an HP 3401A multi-meter; the last recorded value is 1% of the initial one, thus showing that smoke density changes with time. In Fig. 3(a) the image recorded by a standard white-light photo camera after letting smoke in is shown, where the vision is impaired due to the severe scattering of the visible radiation due to the smoke.

In Fig. 3(b) the image obtained by the IR bolometer is displayed. As expected, the thermographic acquisition allows us to see through smoke because the IR light is only slightly scattered by particles due to its longer wavelength (in fact, Rayleigh scattering law predicts low scattering for longer wavelengths). In Fig. 3(c) the IR holographic image is shown. It is evident also that holographic imaging provides clear vision even through smoke.

It is important to note here that, in holographic imaging, the movement of the scattering particles (e.g., soot particles) contributes to reinforce clear vision [11]. Indeed, multiple acquisitions can be reconstructed and averaged to obtain improved images where more detail can be seen, as will be shown in the following section.

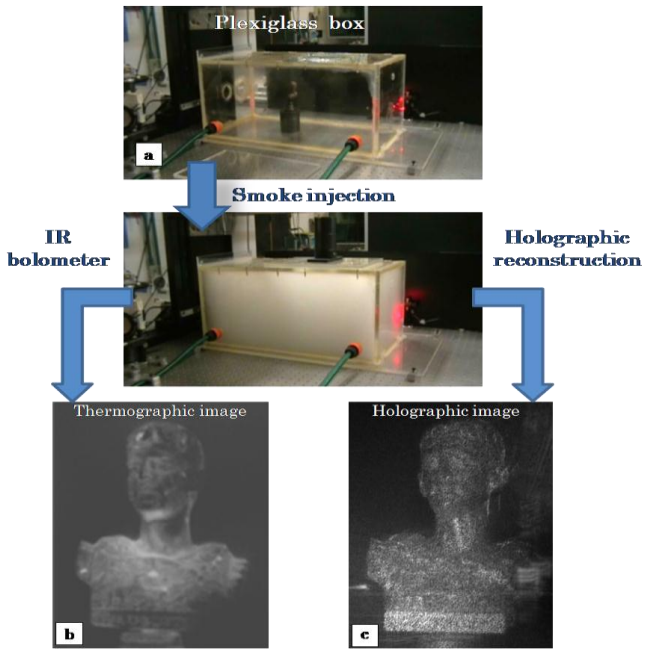

Fig. 3. Target imaging through smoke. (a) Metal object in Plexiglas™ box. Images recorded by a standard white-light photo camera before and after letting smoke into the box. (b) Thermographic imaging of the metal object through smoke. (c) Holographic amplitude reconstruction. This confirms that holography has the same capability of IR imaging to see through smoke.

#181596 - $15.00 USD Received 11 Dec 2012; revised 11 Jan 2013; accepted 15 Jan 2013; published 26 Feb 2013

3.2 Numerical enhancement: speckle reduction by multiple acquisitions

Thanks to numerical techniques, further enhancement of the image quality can be quickly achieved to offer a quasi-real-time display of what is behind flames and smoke. In fact, any kind of imaging system employing a coherent laser source can be degraded by both incoherent and, above all, correlated speckle noise [35,36]. Speckle noise is multiplicative noise that occurs whenever a coherent light hits targets whose roughness varies on the same scale of the employed wavelength. In this case, each detector element records the coherent superposition of a number of different scattering contributions. As they experience microscopically different paths, their phases can be variable and the result of the coherent superposition to the receiver is the typical succession of dark and bright spots known as speckle noise. As a result, the quality of the reconstructed hologram in DH decreases in terms of contrast and pixel resolution. Due to the nature of the problem, it has been tackled in literature relying on statistical approaches. A common way to obtain indications about the speckle extent is to measure the speckle contrast as follows:

$$C = \frac{\sigma}{\mu}, \tag{1}$$

where σ and μ, respectively, denote the standard deviation and the mean amplitude of the image. Furthermore, a punctual measure of the intensity variations due to speckle noise is obtainable by calculating the relative deviation as

$$R_{Dev}(x,y) = \frac{I(x,y)-\bar{I}}{\bar{I}}, \tag{2}$$

where $I(x,y)$ is the intensity of the pixel (x,y) of the reconstructed hologram and $\bar{I}$ its mean intensity calculated over the whole image. In particular, if a cut of a homogeneous part of the original image is chosen, smooth behavior of the plot should be expected. So, any rapid variations and sudden spikes in its shape have to be attributed to speckle in those points where interference has been strongly destructive.

In order to reduce the speckle contrast it is possible to exploit some kind of diversity to obtain holograms from a set of uncorrelated speckle patterns and average them to obtain a multi-look (ML) image. Indeed, it can be shown that the superposition of N statistically independent random variables returns a random variable whose variance is reduced by factor of $1/N$. Hence, the speckle contrast improves a factor of $1/\sqrt{N}$.

Let X_1 and X_2 be two uncorrelated random variables and let

$$Y = aX_1 + bX_2 \tag{3}$$

be a linear combination of them through the coefficients a and b. After easy manipulations it is possible to find that

$$\sigma_Y^2 = a^2\sigma_{X_1}^2 + b^2\sigma_{X_2}^2. \tag{4}$$

Hence, if we denote with

$$\tilde{X} = \frac{1}{N}\sum_{i=1}^{N} X_i \tag{5}$$

the mean of N uncorrelated random variables X_i, each with the same mean $\mu_{X_i} = \mu_X$ and variance $\sigma_{X_i}^2 = \sigma_X^2 \ \forall i = 1,...,N$, the variance of $\tilde{x}$ is given by

$$\sigma_{\tilde{X}}^2 = \frac{1}{N^2}\sum_{i=1}^{N}\sigma_{X_i}^2 = \frac{\sigma_X^2}{N}. \tag{6}$$

#181596 - $15.00 USD Received 11 Dec 2012; revised 11 Jan 2013; accepted 15 Jan 2013; published 26 Feb 2013

Since it results in

$$\mu_{\tilde{X}} = \mu_X , \tag{7}$$

the speckle contrast reduces as

$$C_{\tilde{X}} = \frac{1}{\sqrt{N}} \frac{\sigma_{X_i}}{\mu_{X_i}} = \frac{1}{\sqrt{N}} C_{X_i} , \tag{8}$$

where C_{X_i} denotes the speckle contrast of the single-look (SL) image. Figure 4 shows the holographic reconstruction of the bronze statuette placed into the Plexiglas™ box of Fig. 3. In particular, we acquired a set of holograms after letting smoke into the box, whose effect is to provide a temporal diversity. After proper decimation of the original hologram stack, we obtained a subset of $N = 25$ holograms, and for each of them we performed the numerical propagation after dropping the zeroth diffraction order and the conjugate term arising in the reconstruction process. The reconstructed amplitudes have been averaged and speckle measures have been carried out on both the SL and the ML images in terms of the contrast estimators defined in Eq. (1) and Eq. (2).

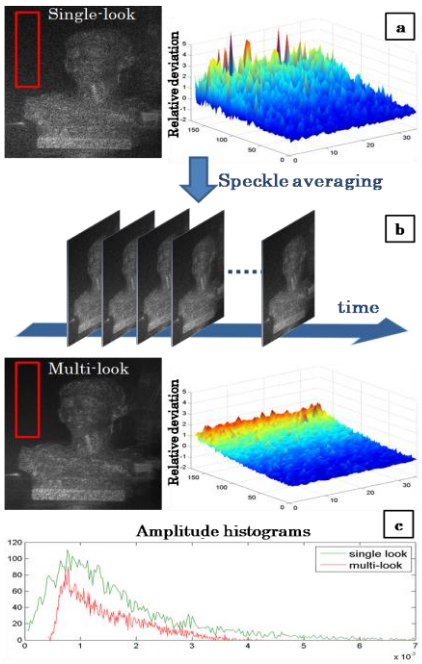

Fig. 4. Target imaging through smoke. (a) Holographic amplitude reconstruction before numerical processing and relative deviation corresponding to a homogeneous cut of the image (red box in figure). (b) Speckle reduction by processing a time sequence of holograms: multi-look reconstruction and relative deviation improvement. (c) Amplitude histograms: comparison between the single look and the multi-look image.

Figure 4(a) shows the SL image and the relative deviation calculated over the homogeneous area corresponding to the red box in Fig. 4. As expected, the noise is responsible for the rapid fluctuations of $R_{Dev}(x,y)$, and the degradation due to the speckle is apparent in the amplitude image as well. In Fig. 4(b) the described procedure is sketched and the resulting ML output is shown. The ML improvement is clearly appreciable in the amplitude image and the relative deviation exhibits a much smoother behavior. This suggests that a significant gain has been achieved in reducing the speckle noise by combining multiple

#181596 - $15.00 USD Received 11 Dec 2012; revised 11 Jan 2013; accepted 15 Jan 2013; published 26 Feb 2013

acquisitions. This claim is confirmed by the measure of speckle contrast, which decreases 12% with respect to the SL image. However, a residual correlation between the employed frames is present, which in turn results in the gap with respect to the maximum theoretical improvement factor, i.e., 20% in the case of N = 25 [see Eq. (8)]. As further validation, we calculated the amplitude histograms in a homogeneous test area of both the SL and the ML reconstructions. As expressed in Eq. (6), the ML gain results in a smaller variance that is apparent in the plots shown in Fig. 4(c).

3.3 Seeing through flames

In the second experiment a digital hologram of objects hidden by a curtain of flames was recorded. The flames were obtained using candles for the case of a small object and a portable mini stove for human-size targets, respectively.

In this way a large portion of the object was covered by flames, impairing vision also with the thermo camera. In fact, in thermographic imaging a lens is used and the whole flame emission is collected and focused on some elements of the IR bolometer, causing saturation and resulting in blind areas [Fig. 5(a)]. On the contrary, holographic recording shows no such problem, allowing us to see through the flames. These capabilities can be explained by some intrinsic features of holography.

First of all, since we used a lensless setup, the IR energy emitted by the flames was not focused but distributed over the whole array of camera pixels, avoiding pixel saturation [see Fig. 5(b)]. Moreover, an interesting property of a hologram, well known since its discovery [37], is that each part of it contains information coming from the whole object, which can be used to reconstruct the entire image [5,6]. Similarly, a small subset of sparse hologram pixels could be used. Therefore, if some of the camera detector is saturated, the corresponding information can be recovered from those elements that have not been affected by saturation. In this way DH is able to provide images of the whole scene with no blind areas, thus getting rid of the flame emission and demonstrating the power of holographic vision. For the same reason, IR-DH allows the vision of objects even if some macro particles, often present in real fire-scenarios, obstruct their direct imaging.

3.4 Human-size holograms

In this section we show that by IR-DH technology it is possible to record digital holograms and visualize (i.e., display on a monitor) objects as large as an adult in a room, as clearly shown by the results in Fig. 6. This would be not possible with visible laser radiation. Just to give an example, with DH at a visible wavelength (532 nm) at a distance of 2 m from the camera, it is possible to successfully record holograms of objects with a maximum size of 15 cm. On the contrary, at the same distance but by using IR radiation, the size increases up to 85 cm. This can be easily explained by considering that the ratio between the wavelength and the pixel size is much more favorable in the case of IR wavelengths. Indeed, in off-axis digital holograms the fringe spacing has to be adjusted in order to satisfy the Whittaker–Shannon sampling theorem. In our experimental test, a plastic mannequin 190 cm tall is used as object [see Fig. 6(a)] and placed at a distance of 300 cm from the detector. The setup is described above and also shown in Fig. 2.

#181596 - $15.00 USD Received 11 Dec 2012; revised 11 Jan 2013; accepted 15 Jan 2013; published 26 Feb 2013

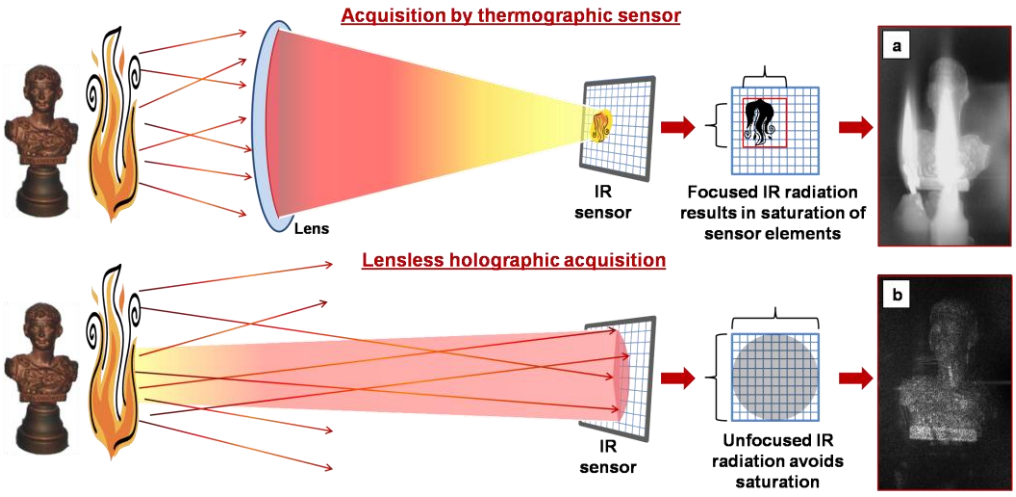

Fig. 5. Imaging of a metal object seen through flames of candles. (a) Thermographic acquisition and corresponding image. (b) Holographic acquisition and amplitude reconstruction. Since no lens is needed, the IR energy is distributed over the whole array of camera pixels, avoiding their saturation.

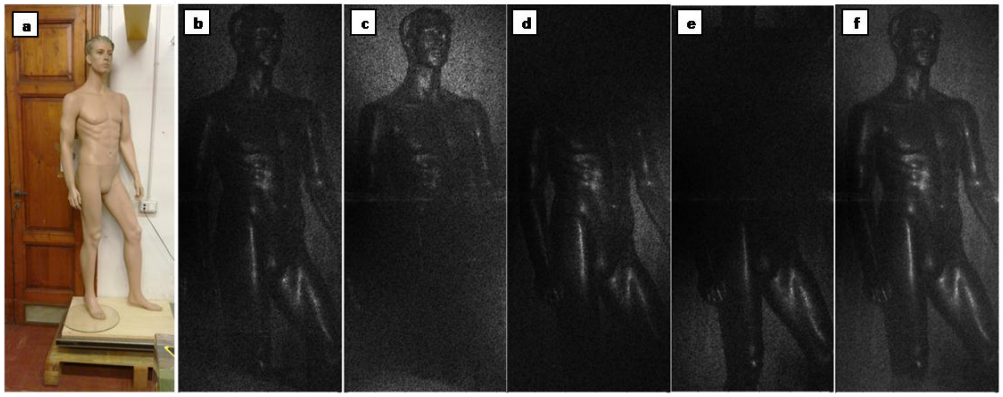

Fig. 6. Holographic capability of imaging human-size objects. (a) White light image of a plastic mannequin 190 cm tall used as a test target. (b-f) Holographic reconstruction of the plastic human-size mannequin. Holograms acquired using the cylindrical lens setup (b), the scanning set-up (c,d,e) and their superposition (f). Digital holography is suited for both small and big human-size targets, like adults in a room.

The laser beam is enlarged by a lens before impinging on the object. However, the object beam dimension is limited by the focusing power of the lens and, therefore, only a portion of the sample can be fruitfully irradiated. In these conditions we cannot take advantage of the increased field of view offered by the longer wavelength because the irradiated area is smaller than the maximum recordable size. To obtain an efficient hologram of the entire object, a cylindrical lens can be inserted in the optical path in order to obtain an elliptical beam, more suitable than the circular one, to illuminate the mannequin. In this way it is possible to exploit more efficiently the available beam energy [see the hologram reconstruction in Fig. 6(b)].

In an alternative configuration a plane mirror driven by two motion control devices can be used to scan the sample surface by the spherical beam, and a sequence of holograms is acquired during the scanning process (the duration of the scan is 30 s). In Fig. 6(c), Fig. 6(d), and Fig. 6(e) the numerical reconstructions of the most significant frames extracted from the video are shown. Finally, in Fig. 6(f) the image obtained is shown superposing the reconstructed frames. The same result can be obtained by the optical reconstruction

#181596 - $15.00 USD Received 11 Dec 2012; revised 11 Jan 2013; accepted 15 Jan 2013; published 26 Feb 2013

(displaying) of the corresponding holograms in a rapid sequence through an SLM-based setup [24].

Figure 7 shows a clear example of the advantages of the proposed technique based on digital holography with respect to thermographic recordings, comparing live human targets imaged through flames. In particular, Fig. 7(a) shows a thermographic image of a man standing up behind a flame whose emission completely occludes the man's body and his face. As a consequence, only arms and hands are visible as they are extended over the flame. Similarly, the white-light images of Fig. 7(b) and Fig. 7(c), respectively, show a live hand and the man with his arms in a different position. Again, the flame emission blinds the detector. However, holographic imaging [Fig. 7(d)] allows us to see the man with the tee shirt and eye glasses clearly, despite the flames in the line of sight of the recording device, and details of the hand are appreciable as well (Media 1). Figure 7(d) has been obtained by means of the ML processing described in Section 3.2. Indeed, in case the line of sight between the target and the recording device is impaired by the presence of a flame whose emission tends to saturate the camera detectors, a set of uncorrelated holograms can be acquired and temporally averaged to achieve an improved ML output. In this case the moving flame itself provides a temporal diversity, as the spatial distribution of the saturated detector elements change in time and the spatial changes of the refractive index due to the flame are time variant as well. Figure 8 shows the improvement achievable by numerical processing. In particular, in the SL image the effect of the saturation is apparent, with dark areas hindering a clear vision of the human target behind the flames, while it becomes visible in the ML reconstruction as the missing information is correctly restored. In this way more details can be appreciated and a post analysis of the scene is possible.

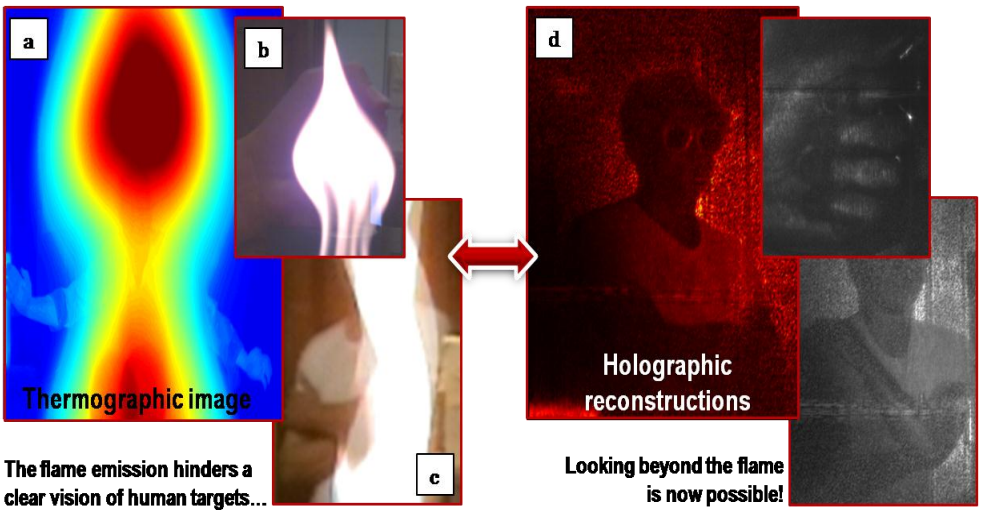

Fig. 7. Imaging of a live human seen through flames. (a) Thermographic image. (Media 1). (b-c) White-light images of a live hand and the man with his arms in a different position. (d) Holographic imaging (Media 1). The flames in this case cover the entire field of view of the recording bolometer.

#181596 - $15.00 USD Received 11 Dec 2012; revised 11 Jan 2013; accepted 15 Jan 2013; published 26 Feb 2013

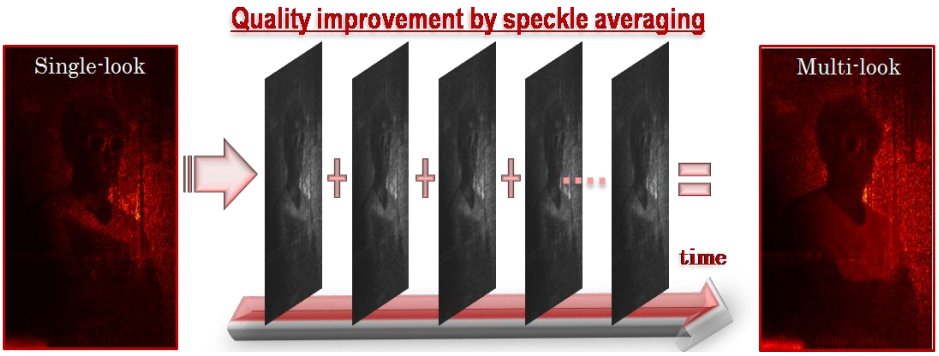

Fig. 8. Imaging of a human target behind a flame. Left: SL holographic reconstruction. Right: ML amplitude image.

4. Conclusions

We claim the holographic imaging technique is useful to see through both smoke and flames apart from their origin, i.e., the type of combustible material. In fact, the output of this interferometric imaging method does not depend on the frequency of the emission spectrum. It is noteworthy that human-size targets can be imaged by DH with IR radiation, thus allowing its application to a wide set of real fire scenes. In these cases, the lensless configuration plays a key role since the detector is not blinded by flame emission, which is the main impediment for thermographic imaging. A further advantage of the proposed technique is that, through a numerical processing of the acquired holograms, is possible to improve *a posteriori* the image quality. This feature could be exploited if, for example, it is necessary for *a posteriori* analysis of a fire scene. We believe the results reported in this paper can open a route for making an imaging technique available that is able to see through fire and possibly to give a completely new chance for saving human lives.

Acknowledgments:

This research was funded by the MIUR (Italian Ministry for Research and University) within the PON project IT@CHA PON01_00980 Italian Technologies for Advanced Application in Cultural Heritage Assets.

#181596 - $15.00 USD Received 11 Dec 2012; revised 11 Jan 2013; accepted 15 Jan 2013; published 26 Feb 2013